Int. J. Electrochem. Sci., 16 **(2021)** Article Number: 211058, doi: 10.20964/2021.10.58

International Journal of
ELECTROCHEMICAL
SCIENCE
www.electrochemsci.org

Anticorrosion Properties of Waterborne Polyurethane Coating Containing Caffeate Anions Intercalated LDH

Haichao Zhao[1],*Wenru Zheng*[1], *Wenjing Liu*[1], *Xin Zhang*[1], *Yue Su*[1,2,*]

[1] Key Laboratory of Marine Materials and Related Technologies, Zhejiang Key Laboratory of Marine Materials and Protective Technologies, Ning--bo Institute of Materials Technology and Engineering, Chinese Academy of Sciences, Ningbo 315201, China
[2] University of Chinese Academy of Sciences, Beijing 100049, China
[*]E-mail: suyue@nimte.ac.cn

Received: 7 July 2021 / *Accepted:* 17 August 2021 / *Published:* 10 September 2021

LDH with caffeate anions intercalation was successfully prepared by acidification of LDH and followed ionic exchange process. Waterborne polyurethane based coatings withouth and with 0.5 wt% LDH and 0.5 wt% caffeate anions intercalated LDH (LCA) were fabricated with the thickness of 70 ± 4 μm. EIS and LEIS were used to characterize the electrochemical and micro-area corrosive behavior of LDH-doped coatings. It displayed that the addition of LDH loaded with caffeate anions improved the impedance of PU from 1.47×10^7 to 3.93×10^7 Ω cm^2 after 30 days immerion in 3.5% NaCl solution. In addition, the micro-area corrosive condition of LCA containing PU is better than that in pure PU and LDH containing PU coating, which could ascribe to the emancipation of intercalated caffeate ions in LDH. The addition of LCA nanohybrids into PU could enhance the barrier performances of PU. Moreover, the excellent ions exchanges ability of LDH could be used to adsorb chloride ions, and the release of caffeate anions could delay the process of corrosion reactions. The synergistic effect of caffeate anions and LDH improves the anti-corrosion performance of waterborne PU.

Keywords: barrier effect, ionic exchange, waterborne polyurethane coating

1. INTRODUCTION

The more and more strict environmental protections regulations have motivated the development of organic coatings using water as the dispersive medium to replace organic solvent. In this respect, one component of water borne polyurethane (WPU) has been widely used as corrosive barrier in anticorrosion coatings due to its ease of synthesis, tunable mechanical properties, as well as weather resistance [1-4]. However, compared solvent borne organic coatings, the waterborne coating suffers from multifarious disadvantages, including inferior corrosion protection performance and low shielding effect and high water permeability due to the presence of emulsifier or water soluble segments in the

polymer chains [5]. This issue has led to many investigative work into improve the anticorrosive performance of waterborne PU based organic coatings [4].

An important advance in the filed of improving the impermeability of WPU is the use of flake-like layered nanomaterial to reduce the moisture or oxygen diffusion through a tortous pathway [4-5]. Many experimental work shows that the anticorrosive properties of the composite coatings are much dependent on the type, dispersion, orientation, aspect ratio and surface functionalities of the layered material [6-9]. For instance, the WPU-based composite coating containing polyetheramine functionalized graphene oxide (GO) was prepared by in-situ polymerization. 0.05wt% PAFG grafted GO obviously improved thermal stability, hydrophobicity, anti-corrosion and mechanical properties of as-prepared coating [10] . Another method using sodium dodecylbenzenesulfonate as noncovalent surfactant to improve the dispersibility of isophorone diisocyanate and N,N-dimethylethanolamine grafted graphene oxide in the WPU coating was reported [11]. Electrochemical impedance spectroscopy analysis and salt spray tests concluded that the addition of 0.3 wt% modified GO significantly improved the anticorrosive performance of composites coatings. Titanate functionalized graphene was incorporated into WPU, and the as-prepared composite coatings on steel substrate were fabricated [12]. It was found that 0.4 wt% graphene layers were self-aligned parallel to the WPU coatings, which fully utilized the high specific surface area of graphene to prevent the electrolyte penetration to the coating, hence affording the superior anticorrosion. Edge hydroxylated hexagonal boron nitride (hBN) was used improve anticorrosive properties of the UV-curable polyurethane coatings, the 0.2 wt% of the hBN loading resulted in a significant lower corrosion current density and more positive corrosion potential [13]. Chitosan and cerium ions loaded montmorillonite were used to enhance the water resistance and barrierprotection of WPU coatings on steel substrates [14]. Results show that pretreatment with chitosan can increase the Ce3+ loading capacity of montmorillonite and improve its dispersion stability in WPU.

Layered double hydroxides (LDHs) are kinds of hydrotalcite-like anionic clays consisting exchangeable interlayer anions, which have been widely used as host to intercalate corrosion inhibitors for ameliorating the anticorrosive and self-healing properties of organic coatings [15-16]. On the other hand, caffeic acid [17], a phenylpropenoid most found in nature, has been proved that an excellent corrosion inhibitor that reduces available cathodic reactions through chemical absorption on the metal substrate. In this experiment, caffeate anions were intercalated into Mg-Al LDH gallieries by anion exchange and nano-reinforcing fillers were used to improve the corrosive protection properties of WPU. The strucutre of LDH and LCA were characterized by scanning electron microscopy, X-ray diffraction, X-ray photoelectron spectroscopy and thermogravimetric analysis, respectively. The WPU based coatings without and with 0.5 wt% LDH were fabricated and the anticorroion performance were investigated by EIS, LEIS and corrosion products analysis.

2. EXPERIMENTS

2.1 Materials

Magnesium nitrate hexahydrate, aluminium nitrate nonahydrate, urea and caffeic acid were purchased from Aladdin Reagent Company. Sodium chloride, sodium hydroxide and hydrochloric acid (36~37 wt%) were bought from Sinopharm Chemical Reagent Co. Ltd. All reagents were directly used

without further purification. Waterborne polyurethane was purchased from Yunda Co., Ltd. Carbon steels with an area of 1 cm×1 cm were polished with 400 , 800 and 1200 C sandpapers and cleaned in ethanol by ultrasonic vibration.

2.2 Nanohybrids Synthesis and Coating Preparation

2 mmol of $Mg(NO_3)_2•6H_2O$, 1 mmol of $Al(NO_3)_3•9H_2O$ and 10 mmol of $CO(NH_2)_2$ were dissolved in 70 mL of deionized water. The reaction was carried out in a tetrafluoroethylene reactor at 140 °C for 8 h. After centrifugation, washing and drying at 60 °C, the product was recorded as LDH, the interlayer anions were carbonate ions.

According to the previous work we reported [18], the interlayer anions could be replaced by acidification and ionic exchanges. 1.0 g of LDH was dissolved in 1 L of 1 M NaCl and 3.3 mM of HCl solutions, the solution was shaked at room temperature for 12 h after nitrogen sweeping, the interlayer anions were replaced with chloride ions. 1M sodium hydroxide solution was dropped into caffeic acid solution to get caffeate anion.The obtained mid-product was dissolved in sodium caffeine solution (the concentration of caffeate anion was 20 times that of chloride ion) to obtained caffeate anions intercalated LDH. In the same way, the products were centrifuged, washed and dried at 60 °C. The final product (caffeate ions intercalated LDH) was recorded as LCA. The ion exchange process is shown in Fig. 1.

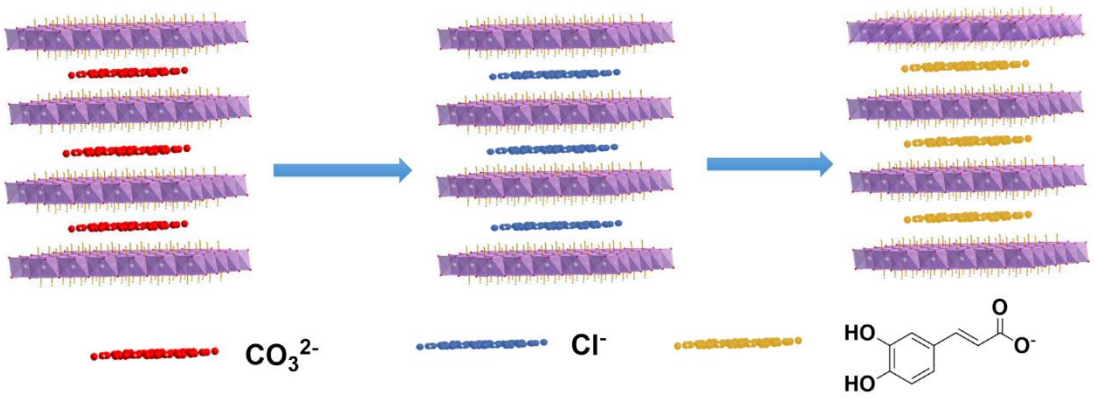

Figure 1. The preparation process of caffeate anions intercalated LDH

The nanohybrids LDH and LCA were (0.5 wt%) dissolved in 5 mL of ethanol respectively. Then, a certain amount of polyurethane was added into the above solutions and stirred vigorously for 20 mins. Q235 steels were polished with 400, 800 and 1200 C sandpapers respectively, and the substrates were cleaned by ultrasonic treatment in ethanol and dried by vacuum oven. The mixture made by coating rod on Q235 steel (1cm×1cm) had a thickness of 70 ± 4μm.

2.3 Characterization of nanohybrids

The morphologies of LDH and LCA were characterized by scanning electron microscopy (SEM, S4800). The organic groups of LDH and LCA were charactered by FTIR from 4000 to 500 cm^{-1}. The galleris distances of LDH and LCA were characterized by X-ray diffraction (XRD, D8 ADVANCE DAVINCI). XRD patterns were got through using monochromatic Cu Kα radiation in the range of 5-70° at a rate of 3 °/min. X-ray photoelectron spectroscopy (XPS, axis ultra, DLD) was used to detect element composition and relative mass concentrations. The thermal properties of LDH and LCA were measured by thermogravimetric analysis (Diamond TG/DTA).

2.4 Characterization of nanohybrids coatings and corrosion products

The morphologies of LDH and LCA nanohybrids coatings were measured by SEM (S4800). The distributions of LDH and LDH-Cdot nanohybrids were also characterized by TEM. The corrosion morphologies and elements distributions of Q235 steels were characterized by SEM (FEI Quanta FEG 250).

2.5 Electrochemical measurement

Electrochemical workstation (CHI-660E) was used to characterize the long-term anticorrosive properties of nanohybrids coatings in 3.5 wt% NaCl solution. Saturated calomel electrode (SCE) and platinum plate were used as a reference electrode and counter electrode, respectively. Electrochemical impedance spectroscopy (EIS) measurement was carried out in the frequency range from 10^5 Hz to 10^{-2} Hz with sinusoidal disturbance of 20 mV amplitude. EIS results were analyzed by Zview software. The micro-electrochemical corrosive behaviors of the nanohybrids coatings were detected by localized electrochemical impedance spectroscopy (LEIS) on Versa SCAN Micro-Scanning Electrochemical Workshop (AMETEK, USA). During the test, the amplitude was 50 mV, and the test frequency was 10 Hz.

3. RESULTS AND DISCUSSION

3.1. Characterization of LDH and LCA

As shown in Fig. 2a and 2b, LDH is a typical hexagonal structure with lateral size of 1-2 μm. After acidification and ionic exchange, the surface morphology of LCA still keeps the hexagonal structure. FTIR was carried out to characterize the chemical properties of LDH and LCA. As displayed in Fig. 2c, the peaks near 3440 cm^{-1} belong to O-H stretching vibration of the interlayer H_2O and structural OH groups [1]. The peak at 1644 cm^{-1} belongs to the alkenyl C=C stretching vibration, the peak at 1626 cm^{-1} characterizes the deformation of O–H and the peak at 1215 cm^{-1} can be attributed to vibration of C–O (epoxy) [19]. According to previous literature, the characteristic peak at 1353 cm^{-1}

represents the vibrational absorption of interlayer CO_3^{2-} (v3) [18]. The peaks at 1162 and 1119 cm^{-1} correspond to C-OH stretching vibration. The peak at 974 cm^{-1} ascribes to =C-H out-plane bending vibration. The sharp bands around 781, 683 and 552 cm^{-1} are caused by various lattice vibrations associated with metal hydroxide sheets [20-23]. This means caffeate anions have been adsorbed on LDH.

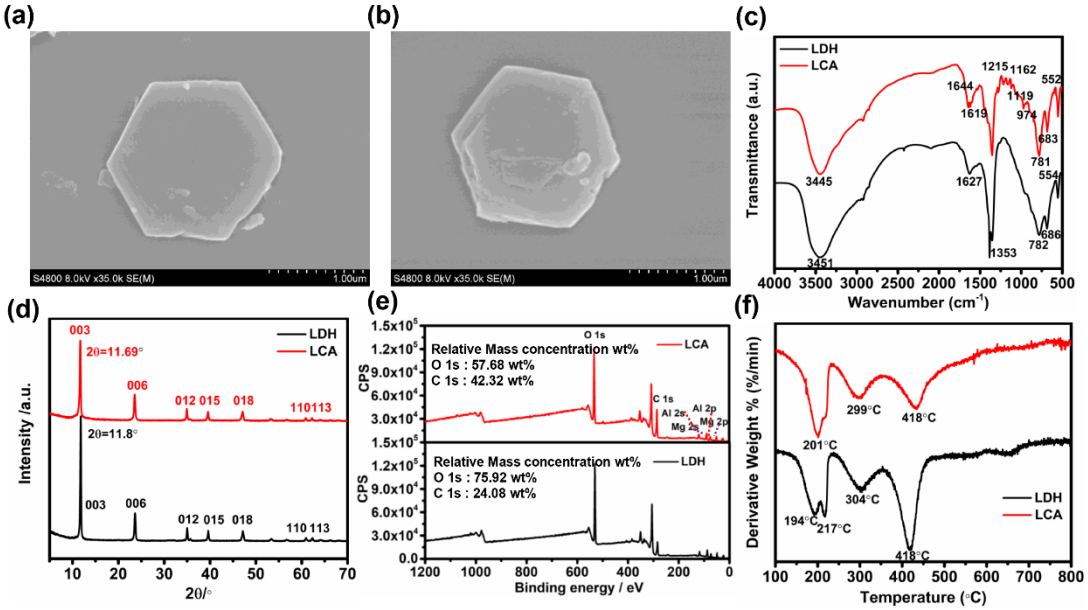

Figure 2. (a-b) SEM scanning figures of LDH and LCA. (c) FTIR spectrum of LDH and LCA. (d) XRD patterns of LDH and LCA. (e) XPS spectrum of LCA. (f) Thermogravimetry curves of LDH and LCA.

Fig. 2d shows the XRD patterns of LDH and LCA, in which (003) and (006) planes are the characteristic diffraction peaks of hydrotalcite clay [24-25], (012), (015), (018), (110) and (113) planes ascribe to the non-basement reflection [26]. The volume and stacking mode of interlayer anions determine the interlayer spacing of LDH. After acidification and ionic exchanges, the XRD characteristic peaks of LDH are shifted to low degrees, especially the (003) crystal plane. According to Bragg equation, the layer space of LCA is 0.756 nm, while the layer space of LDH is 0.749 nm [18, 27]. The change of galleries distances of LDH also confirmed that caffeate anions had been inserted into LDH gallery.

Fig.2f exhibits thermogravimetry curves of LDH and LCA, the carbon content of LCA have been improved significantly in Fig. 2e. As shown in Fig. 2e, the relative mass concentration of carbon element was 24.08 % in LDH, and the relative mass concentration of oxygen element was 75.92 % in LDH. While the relative mass concentration of carbon element was improved to 42.32 % in LCA, the relative mass concentration of oxygen element was decreased to 57.68 % in LCA. This phenomenon indicates that caffeate anions have been adsorbed on the gallery of LDH.

As shown in Fig 2f, three weight loss steps occurred during the thermal decomposition of LDH and LCA. The physiosorbed water on the surface of LDH and the intercalated water in the interlayer galleries were removed at the temperature range of 100-200 °C, the decomposition temperatures of

carbonate ions and caffeate ions are at the ranges of 200-300 °C. The third weight loss step (400–500 °C) corresponds to the de-hydroxylation of the brucite-like layers and the combustion of the decomposed nanohybrids [28].

3.2 Characterization of LDH based composite coating

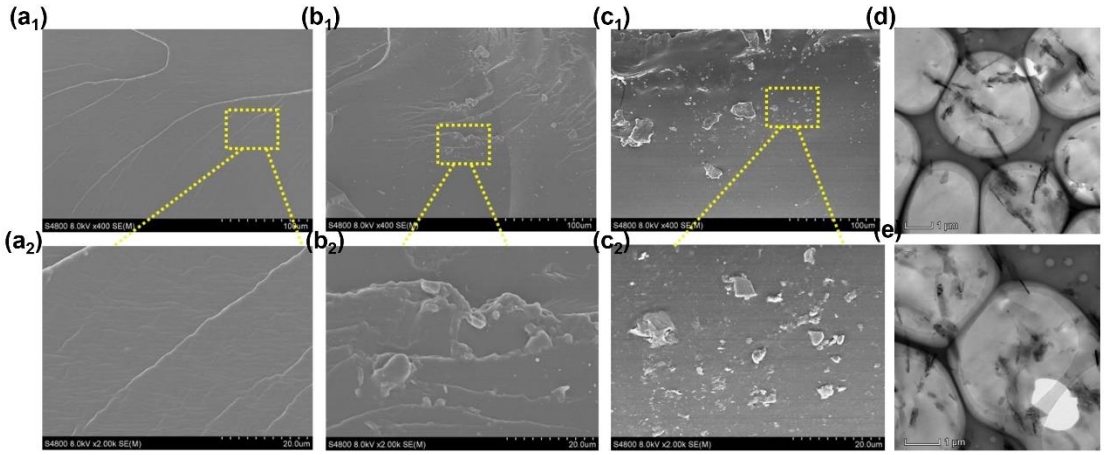

Figure 3. The brittle section information of (a_1-a_2) pure PU, (b_1-b_2) LDH PU and (c_1-c_2) LCA PU by SEM. The TEM images of (d) LDH PU and (e) LCA PU.

The distribution of two-dimensional nanomaterials in polymer matrix is the most important parameter influencing coating protection performance [29-30]. SEM was used to observe the distributions of nanohybrids in the fracture sections of PU coatings. As shown in Fig. 3a, the oblique stripes can be produced by rapid cooling in the liquid nitrogen environment, the smooth fracture surface would not stop microcracks expanding in pure PU. Thus, added nanohybrids can prevent the propagation of microcracks. As shown in Figure 3b_1, 3b_2, 3c_1, 3c_2, 3d, 3e, LDH and LCA nanohybrids are dispersed in PU resin to prevent the microcracks spreading. The dispersion of different nanohybrids is dependent on the compatibility between resin and nanohybrids. The hydrogen groups on the surfaces of LDH and LCA can enhance the dispersion of nanohybrids.

3.3 Barrier performance of nanohybrids coatings

Corrosion resistance of nanohybrids coatings were measured by EIS in 3.5 wt% NaCl solution. As shown in the Fig. 4d, with the increase of immersion time , the OCP of pure PU coating decreased gradually, but the OCP of LDH PU and LCA PU are higher than that in pure PU, which indicating that the addition of LDH and LCA nanohybrids can improve the OCP of PU coatings. When soaked for 720 h, the OCP of LCA-PU coating was -0.0368 V, which was higher than that of pure PU (-0.0744V) and LDH-PU coating (-0.066 V), demonstrating the addition of LCA enhances the shielding effect of coatings.

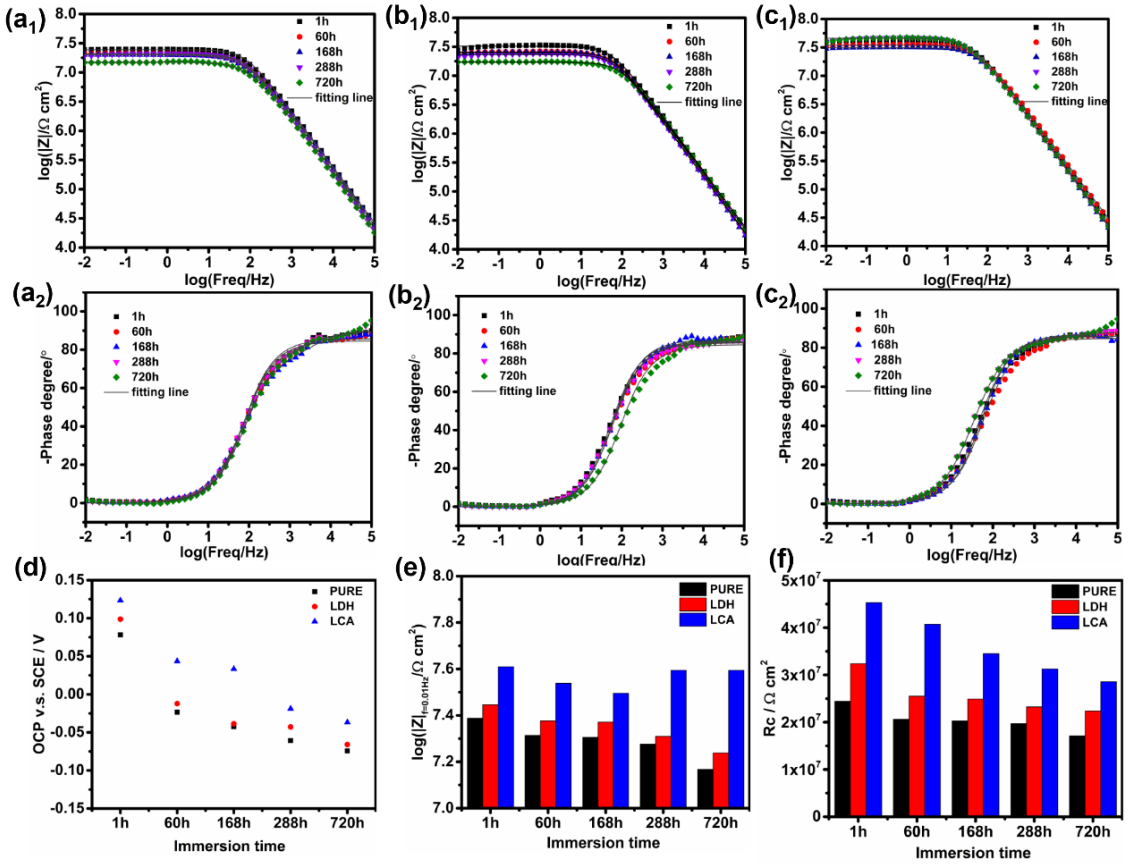

Figure 4. The Bode impedances and phase angles plots of (a_1-a_2) pure PU, (b_1-b_2) LDH PU and (c_1-c_2) LCA PU in different immersion times. (d) Open circuit potential of pure PU, LDH PU and LCA PU with time.(e) Log value of impedance at 0.01Hz ($\log(|Z|_{0.01Hz})$)with time. (f) the resistances of the coating over time.

As shown in Fig. 4a_1, b_1, c_1, the impedances at 0.01Hz of different coatings are decreased, as well as the protective performance of different coatings are gradually weakened as the soaking time increasing. The impedances at 0.01Hz show that LCA-PU coating keeps the highest impedance modulus, and the order of coatings impedances is $|Z|_{f=0.01Hz}$ (LCA PU) > $|Z|_{f=0.01Hz}$ (LDH PU) > $|Z|_{f=0.01Hz}$ (pure PU). For being soaked 1day, the $|Z|_{f=0.01Hz}$ of LCA-PU was 4.07×10^7 Ω cm^2, while the $|Z|_{f=0.01Hz}$ of LDH PU was 2.79×10^7 Ω cm^2 and the $|Z|_{f=0.01Hz}$ of pure PU was 2.44×10^7 Ω cm^2. After being added LCA, the impedance at 0.01Hz of LCA PU is significantly improved. After 30 days immersion, the $|Z|_{f=0.01Hz}$ of LCA PU was decreased to 3.93×10^7 Ω cm^2; while the $|Z|_{f=0.01Hz}$ of LDH PU was decreased to 1.73×10^7 Ω cm^2 and the $|Z|_{f=0.01Hz}$ of PU was decreased to 1.47×10^7 Ω cm^2. As displayed in Fig. 4a_2, b_2, c_2, only one time constant appears in the Bode phase diagrams of all PU coatings after 30 days of immersion. These phenomena indicate that the electrochemical processes on these samples are mainly controlled by the coating resistance of the coating [31], and the equivalent circuit of pure PU, LDH PU and LCA PU in Fig. 5. Meanwhile, it is found that the anticorrosion property of coatings is decided by the type of coating and the shielding effect of the nanohybrids.

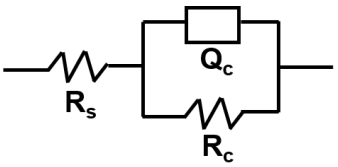

Figure 5. The equivalent circuit of pure PU, LDH PU and LCA PU in different immersion time.

Fig. 4e shows the impedance modulus changes with time at 0.01Hz for the hybrids coatings. The $|Z|_{f=0.01Hz}$ is relative to the barrier performance of coating. Obviously, $|Z|_{f=0.01Hz}$ values showed the time dependence of all coated samples is similar and decreases with the immersion time.It is noted from Fig. 4f that the $|Z|_{f=0.01Hz}$ value of pure PU decrease from 2.44×10^7 to 1.47×10^7 Ω cm^2 during 30 days immersion. Wang et al. found that the $|Z|_{f=0.01Hz}$ values of epoxy coatings below 10^7 Ω cm^2 could not prevent the corrosion reaction of metal substrates under alternating hydrostatic pressure [32-33]. Therefore, pure PU was closely to the coating failure. The coatings with nanohybrids keep higher $|Z|_{f=0.01Hz}$ value. The $|Z|_{f=0.01Hz}$ value of LCA PU was 3.93×10^7 Ω cm^2 for 30 days immersion. Thus, the protective performance of LCA PU is improved significantly. The coating resistances were obtained from the equivalent circuits. As shown in Fig. 4f, the resistance of pure PU was always lowest than any other coatings, which is consistent with the tendency of $|Z|_{f=0.01Hz}$. Fig. 4f depicts the resistance of LCA PU always keeps the highest value, which indicates that nanohybrids LCA PU can effectively improve the barrier performance of epoxy.

3.4 Micro-area corrosive behavior of scratched coatings.

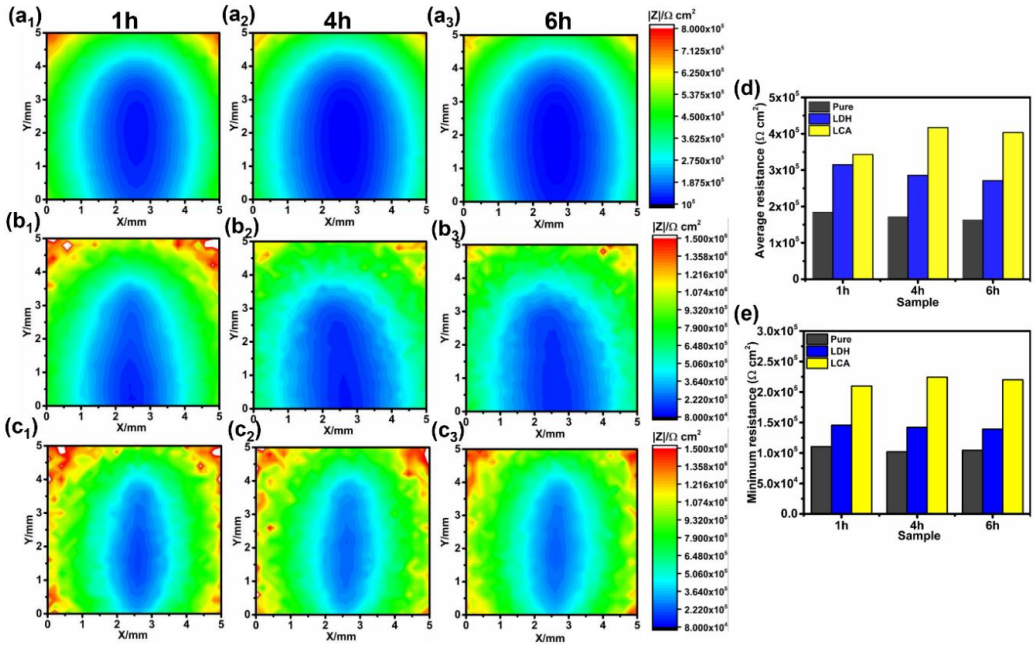

Figure 6. Local electrochemical impedance spectroscopy of scratched coatings (a_1-a_3) pure PU, (b_1-b_3) LDH PU and (c_1-c_3) LCA PU) in 3.5wt% NaCl solutions over times. (d) The average impedance of scratched area and (e) minimum impedance of scratched areacchange with being soaked time.

To deeply study nanohybrids coatings mechanism, artificial scratches about 4 mm long were made on the surface of the nano-hybrid coatingthe artificial scratches were made on the surfaces of the nanohybrids coatings and the micro-area corrosive behavior was evaluated by LEIS. The scratched PU coatings were immersed in 3.5 wt% NaCl solution and measured after 1, 4 and 6 h immersion. As shown in Fig. $6a_1$-$6c_3$, all the coatings are presenting that the resistances of scratch areas are lower than the intact parts. all coatings showed that the resistance of the scratched area was lower than that of the complete part [34]. For pure PU and LDH PU coatings, the defective areas are easily corroded by corrosive electrolytes. As the immersion time progresses, the scratched areas on pure PU and LDH PU coatings were severe corroded, the corrosive areas became larger. Oxygen, water and corrosive electrolyte could permeate into the internal of coatings through the scratches, and loose iron hydroxide cannot inhibit corrosion, so the resistances of the coatings are reduced gradually. Because pure PU lacked nanofillers, the resistances of pure PU coating were lowest after being soaked for 6 h immerison. For LCA PU coating, the resistances of scratched area were higher than that in pure and LDH PU coatings. This phenomenon is mainly owing ascribes to the coupling effect between caffeic acid ions and iron ions to accelerate the formation of passivation film. Compared Fig. $6c_1$, Fig. $6c_2$ with Fig. $6c_3$, it is found that the corrosion area decreases gradually, which means caffeic acid ions are coupled with iron ions to decrease the corrosion progress. Compared with other samples, the corrosion condition of LCA PU coating is leastlightest. These phenomena indicate that caffeic acid ions can absorb on the metal substrate to accelerate the formation of passivativepassivation layers and reduce the progress of corrosion reaction.

Fig. 6d and 6e show the average and minimum scratch resistances of the entire scratched area. As shown in Fig. 6d, the average resistances of LCA PU coating are higher than the average resistances of pure PU and LDH PUwhich are consistent with the LEIS figure. In Fig. 6e, the minimum resistances of LCA PU coating also keep highest after 6 h immersion.This phenomenon reveals caffeate anions can lower down the corrosion progressand protect metal substrate from being corroded by electrolytes.

3.5 Corrosion product analysis

After being soaked in 3.5 wt% NaCl solution for 30 days, the PU coatings were taken away from Q235 carbon steel substrates and cleaned with deionized water two times to eliminate the contaminants. As shown in Fig. 7, the surface morphologies of substrates and the elements distributions of corrosion products were analyzed to evaluate the corrosion condition of metal substrates. Compared with three different metal substrates, it is found that the metal surface of pure PU is tough and full of bumps with different sizes. The uneven surface is mainly made up of Fe, O and Cl. After being added LDH, the barrier effect it provides can reduce the infiltration of oxygen. The iron content of the metal substrate is increased and the oxygen content is decreased. Caffeic acid ions could absorb on the surface of metal substrate to accelerate the formation of passivation film. Therefore, the surface of LCA PU coating become flatter and the relative content of Fe is the highest. In short, LCA nanohybrids can not only enhance the barrier performance of PU but adsorb on the metal surface to prevent metal corrosion. Raman spectroscopy was used to analyze the chemical composition of corrosion products. The corrosion products of pure PU coating are made up of γ-FeOOH (213 cm^{-1}, 1325 cm^{-1}) [35], α-FeOOH (276 cm^{-1})

[36], β-FeOOH (394 cm^{-1}) [37-38], while the compositions of LDH PU are mainly composed of Fe_2O_3 (298 cm^{-1}) and Fe_3O_4 (535 cm^{-1}, 667 cm^{-1}) [39-40]. Compared with LDH PU system, the relative content of Fe_3O_4 (535 cm^{-1}, 667 cm^{-1}) are enhanced apparently, which prove that the release of caffeate anions could promote the passivation of metal substrate and prevent pitting corrosion from further aggravating.

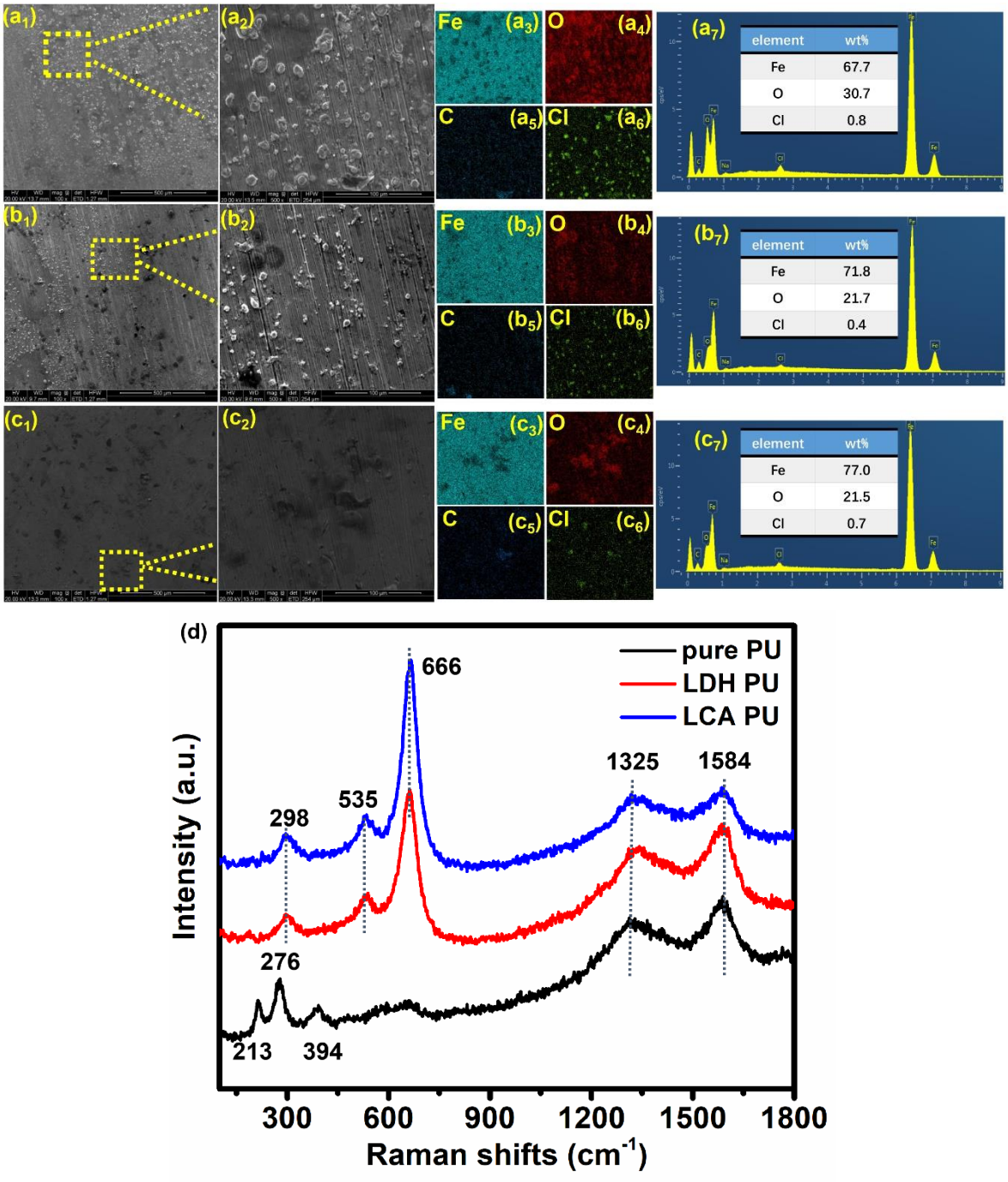

Figure 7. The surface morphologies and elements analysis of metal substrates after being removed (a) pure PU, (b) LDH PU and (C) LCA PU. (d) Raman spectrum of corrosion products.

3.6 Protection mechanism of nanohybrids PU coatings

Polyurethane coatings are immersed in 3.5 wt% NaCl for a long term, chloride ions, water and oxygen molecules continuously infiltrate into the coatings, which easily lead to micro-cracks and micro-holes. In order to retard the process of corrosion reactions, adsorbed caffeate anions were released from LDH interlayer, the oxygen group of organic inhibitors can provide a lone pair of Fe^{2+} cations with an empty 3d orbital, resulting in the chelation between these compounds [41], this action could retard the corrosion reaction. In short, the nanohybrids could fill the coating porosities and cavities and provides effective active anti-corrosion effect.

4. CONCLUSION

LDH with caffeate anions intercalation was successfully prepared by acidification and followed ion exchanging process. Waterborne PU without and with 0.5 wt% LDH and 0.5 wt% LCA were fabricated. EIS and LEIS studies show that LDH's lamella structure improves the barrier performance of PU, the released caffeate anions can interact with Fe^{2+} cations generated on the anodic regions, resulting in the formation of passivation film. Barrier performance and active anti-corrosion make LCA as a promising and environmentally friendly nano-filler for anti-corrosion applications.

References

1. A.Mohammadi, M. Barikani, A.H. Doctorsafaei, A.P. Isfahani, E. Shams and B. Ghalei, *Chem. Eng. J.*, 349 (2018) 466-480.
2. J. Li, L. Gan, Y. Liu, S. Mateti, W. Lei, Y. Chen and J. Yang, *Eur. Polym. J*., 104 (2018) 57-63.
3. X. Li, P. Bandyopadhyay, T. Kshetri, N.H. Kim and J.H. Lee, *J. Mater. Chem*. A, 6 (2018) 21501-21515.
4. L.C. Jing, T. Wang, W.W. Cao, J.G. Wen, H. Zhao, Y.J. Ning, X.T. Yuan, Y. Tian, L.H. Teng and H.Z. Geng, *Prog. Org. Coat*., 146 (2020) 105734.
5. J. Luo, J. Wang, S. Wen, D. Yu, Y. Wu and K. Sun, *J. Coat. Technol. Res*., 15 (5) (2018) 1107–1115.
6. F. Wang, L. Feng and G. Li, *Polymers,* 10 (2018) 1406.
7. A.Mirmohseni, M. Akbari, R. Najjar and M. Hosseini, *J. Appl. Polym. Sci*. 136 (2018) 47082.
8. L. Hou, M. Zhou and S. Wang, *Diamond Relat. Mater*., 90 (2018) 166-171.
9. F. Zhang, W. Liu, L. Liang, S. Wang, H. Shi, Y. Xie, M. Yang and K. Pi*, Colloids Surf.*, A, 591 (2020) 124565.
10. F. Zhang, W. Liu, L. Liang, M. Yang, S. Wang, H. Shi, Y. Xie and K. Pi, *Diamond Relat. Mater*., 109 (2020) 108077.
11. J. Wen, W. Geng, H. Geng, H. Zhao and L. Jing, *ACS Omega*, 4 (2019) 20265−20274.
12. Y. Li, Z. Yang, H. Qiu, Y. Dai, Q. Zheng, J. Li and J. Yang, *J. Mater. Chem*. A, 2 (2014) 14139-14145.
13. H. Liu, H. Zhang, C. Peng, S. Ren, C. Yuan, W. Luo, G. Chen, F. He and L. Dai, *J. Coat. Technol. Res.,* 16 (2019) 1479-1492.
14. Q. Mo, W. Li, H. Yang, F. Gu, Q. Chen and R. Yang, *Prog. Org. Coat*., 136 (2019) 105213.
15. Y. Yang, L. Xiong, X. Huang, Q. Shi and W.D. Zhang, *Composites Communications*, 13 (2019)

112-118.
16. A.Mohammadi, D. Hosseini, A.P. Isfahani, Z. Dehghani and E. Shams, *Polym. Adv. Technol*., (2021) 1-15.
17. F.S. de Souza and A. Spinelli, *Corros.Sci*., 51 (2009) 642-649.
18. Y. Su, S. Qiu, D. Yang, S. Liu, H. Zhao, L. Wang and Q. Xue, *J. Hazard. Mater*., 391 (2020) 122215
19. M. Meshki, M. Behpour and S. Masoum, *Anal. Biochem*., 473 (2015) 80-88.
20. F. Liu, L. Zhou, L. Tao, L. Qian, G. Yu and S. Deng*, Chemosphere*, 253 (2020) 126704.
21. A.Baykal, H. Erdemi and M. Amir, *J. Inorg. Organomet. Polym. Mater*., 26 (2015) 190-196.
22. A.Belay, H.K. Kim and Y.H. Hwang*, Luminescence*, 31 (2016) 654-659.
23. A.Barra, O. Lazar, A. Pantazi, M.J. Hortiguela, G. Otero-Irurueta, M. Enachescu, E. Ruiz-Hitzky, C. Nunes and P. Ferreira, *Nanomaterials* (Basel), 11 (2021) 732.
24. M.L. Zheludkevich, S.K. Poznyak, L.M. Rodrigues, D. Raps, T. Hack, L.F. Dick, T. Nunes and M.G.S. Ferreira, *Corros. Sc*., 52 (2010) 602-611.
25. J. Tedim, A. Kuznetsova, A.N. Salak, F. Montemor, D. Snihirova, M. Pilz, M.L. Zheludkevich and M.G.S. Ferreira, *Corros. Sci*., 55 (2012) 1-4.
26. Y. Cao, S. Dong, D. Zheng, J. Wang, X. Zhang, R. Du, G. Song and C. Lin, *Corros. Sci.,* 126 (2017) 166-179.
27. B. Wu, J. Zuo, B. Dong, F. Xing and C. Luo, *Appl. Clay Sci*., 180 (2019) 105181.
28. M. Wei, X. Xu, J. He, Q. Yuan, G. Rao, D.G. Evans, M. Pu and L. Yang, *J. Phys. Chem. Solids*, 67 (2006) 1469-1476.
29. M. Cui, S. Ren, S. Qin, Q. Xue, H. Zhao and L. Wang, *Corros. Sci*., 131 (2018) 187-198.
30. X. Luo, J. Zhong, Q. Zhou, S. Du, S. Yuan and Y. Liu, *ACS Appl. Mater. Interfaces*, 10 (2018) 18400-18415.
31. B. Ramezanzadeh, S. Niroumandrad, A. Ahmadi, M. Mahdavian and M.H.M. Moghadam, *Corros. Sci.,* 103 (2016) 283-304.
32. L. Liu, Y. Cui, Y. Li, T. Zhang and F. H. Wang, *Electrochim. Acta*, 62 (2012) 42-50.
33. Y. Liu, J. W. Wang, L. Liu, Y. Li and F. H. Wang, *Corros. Sci*.,74 (2013) 59-70.
34. Y. Su, S. H. Qiu, J. Y. Wei, X. B. Zhu, H. C. Zhao, and Q. J. Xue, *Chem. Eng. J*. 426 (2021) 131269.
35. Ph. Colomban, S. Cherifi, and G. Despert, *J. Raman Spectrosc*., 39 (2008) 881-886.
36. X. Zhang, K. Xiao, C. F. Dong, J. S. Wu, X. G. Li, and Y. Z. Huang, *Eng. Failure Anal*. 18 (2011) 1981-1989.
37. R. Elemuren, R. Evitts, I. N.A. Oguocha, G. Kennell, R. Gerspacher, and A. G. Odeshi, *Tribol. Int*., 142 (2020) 105989.
38. S. J. Oh, D. C. Cook, and H. E. Townsend, *Hyperfine Interact*., 112 (1998) 59-66.
39. D. Bersani, P. P. Lottici, and A. Montenero, *J. Raman Spectrosc*., 30 (1999) 355-360.
40. H.C.Z, X. B. Zhu, L.P. Wang, and Q. J. Xue, *Chem. Eng. J*. 410 (2021) 128301.
41. Z. Sanaei, G. Bahlakeh, and B. Ramezanzadeh *J. Alloys Compd*., 728 (2017) 1289-1304